Simultaneous reconstruction of sources and scatterers in a three-dimensional stratified ocean waveguide

Keji Liu* Dinghua Xu†

Abstract. In this work, we extend the direct method in [26] to identify the marine sources and scatterers simultaneously from the far-field pattern in a stratified ocean waveguide. The proposed approach is essentially direct and does not involve any optimizations, solution procedures or matrix inversions, thus computationally rather efficient and simple. Some numerical simulations are carried out to exhibit the robustness and effectiveness of the proposed method in the reconstruction procedure. The extended direct method can not only identify the sources in different locations but also can reconstruct the scatterers in different shapes and positions, therefore it can be considered as an efficient numerical approach for providing reliable estimates of the marine inhomogeneities in the marine acoustics.

Key words. Stratified ocean waveguide, inverse scattering, direct method, far-field pattern.
MSC classifications. 35R30, 41A27, 76Q05.

Dedicated to Professor Robert Pertsch Gilbert on the occasion of his 90th Birthday

1 Introduction

Pioneer work of Professor R. Gilbert, Professor Y. Xu and coauthors. The forward and inverse scattering problems of underwater acoustics have received great attention in recent years since they have wide applications in identifications of mineral deposits, wreckages, submarines, reef and submerged oil etc. Professor R. Gilbert as one of the great mathematician who started the investigation of this problem in the 1980s, and he mentioned it in his biography [8] in 2012:"Bob became interested in underwater acoustics after a summer at the Naval Underwater Systems Center in New London, Connecticut. Shortly after Xu arrived in Delaware, Bob received a research grant on underwater acoustics from Sea Grant. He put Xu into the grant and directed him to get into this challenging area of applied and computational mathematics. This started a collaboration on direct and inverse scattering problems in marine acoustics lasting more than twenty years." In the past forty years, Professor R. Gilbert, Professor Y. Xu and coauthors have obtained lots of impressive results for the scattering problems of ocean acoustics.

Background and description. One of the popular models employed for acoustic waves in the shallow ocean is the waveguide $\mathbb{R}^3_h := \mathbb{R}^2 \times [0, h]$ bounded by two parallel planes Γ_- and Γ_+, see Figure 1(a) for demonstration. In this model, we assume the ocean waveguide has a pressure released surface and a perfectly rigid seabed, on which the Dirichlet condition and the Neumann condition are respectively posed, namely,

$$u = 0 \ \text{ on } \ \Gamma_+ \quad \text{and} \quad \frac{\partial u}{\partial \nu} = 0 \ \text{ on } \ \Gamma_-, \tag{1.1}$$

where u stands for the total acoustic pressure field which consists of the incident field u^i and the scattered field u^s, ν represents the normal vector, $\Gamma_+ := \{x = (x_1, x_2, x_3) \in \mathbb{R}^3_h : x_3 = h\}$ means the ocean surface

*School of Mathematics, Shanghai University of Finance and Economics, 777 Guoding Road, Shanghai 200433, P. R. China. (liu.keji@sufe.edu.cn; kjliu.ip@gmail.com).

†School of Sciences, Zhejiang Sci-Tech University, Hangzhou 310018, P. R. China; School of Mathematics, Shanghai University of Finance and Economics, 777 Guoding Road, Shanghai 200433, P. R. China. (dhxu6708@zstu.edu.cn; dhxu6708@mail.shufe.edu.cn).

and $\Gamma_- := \{x = (x_1, x_2, x_3) \in \mathbb{R}^3_h : x_3 = 0\}$ is the seabed. It is worth mentioning that Prof. Gilbert and his co-authors also consider an elastic seabed (or a poroelastic seabed) instead of the rigid one.

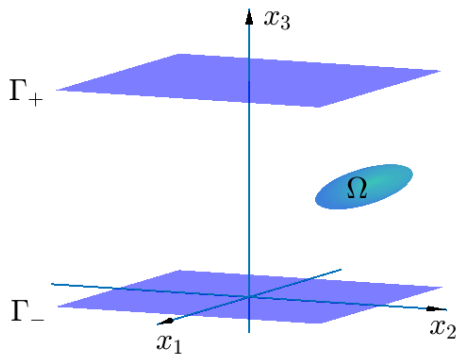

Figure 1: *The demonstrations of one-layered waveguide.*

Due to the special geometry of waveguide, the sound waves may be trapped by acoustic ducts and caused to propagate horizontally, and only a few wave modes can propagate in long distance while the others decay exponentially. Therefore, the scattering problems in the shallow ocean waveguide are much harder than the one in a homogeneous space. Nevertheless, Prof. Gilbert, Prof. Xu and coauthors study the scattering problems of the one-layered waveguide and have obtained many impressive results, which include the Green's function [6, 7, 12], the well-posedness analysis and the uniqueness analysis [6, 13], the numerical methods and analysis for the scattered fields [4, 9, 14, 16, 18, 27], the effective reconstruction methods for marine scatterers [5, 20, 21, 34], the efficient reconstruction algorithms for marine sources [35, 36], the seamount problems [6, 17] and references therein.

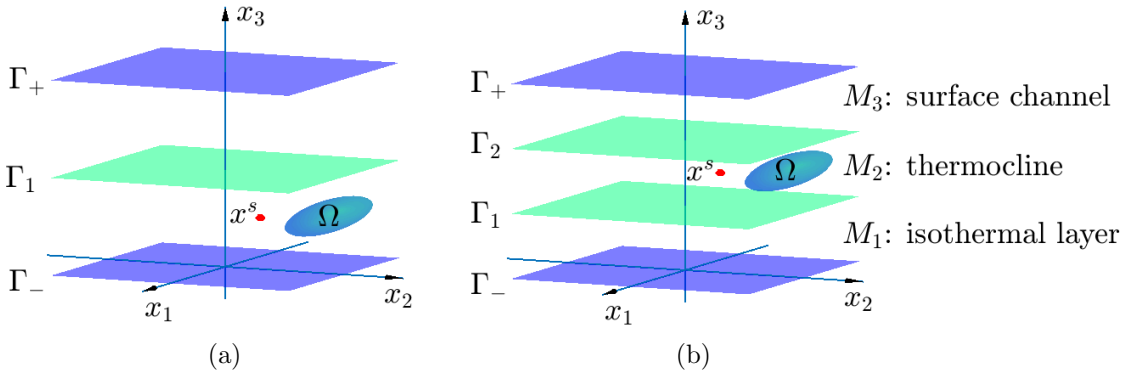

Figure 2: *The demonstrations of (a) two-layered waveguide and (b) three-layered waveguide.*

In order to describe the general ocean environment, a stratified waveguide is introduced since the ocean is approximately horizontally stratified, for instance, we refer to Figures 2(a) and (b) for the demonstrations of the two-layered waveguide and the three-layered waveguide respectively. In this model, the continuous conditions are posed on the interface $\Gamma_i\,(i = 1, 2)$ of the adjacent layers, say,

$$\rho_+ u_+ = \rho_- u_- \quad \text{and} \quad \frac{\partial u_+}{\partial \nu} = \frac{\partial u_-}{\partial \nu}, \tag{1.2}$$

where ρ means the density, and subscripts $+$ and $-$ represent the variable x_3 approaching the interface $\Gamma_i := \{x = (x_1, x_2, x_3) \in \mathbb{R}^3_h : x_3 = h_i\}\,(i = 1, 2)$ from upward and downward respectively. The stratified waveguide is a simple but reasonably realistic model for studying the effect of the underwater sound wave propagation, and we would like to mention that the three-layered waveguide is more reliably than the two-layered one from the fact that the ocean consists of the isothermal layer M_1, the thermal layer M_2

and the surface channel M_3. And the three layers are expressed as follows:

$$\begin{aligned} M_1 &:= \Big\{x = (x_1, x_2, x_3) \in \mathbb{R}^3_h : 0 < x_3 < h_1\Big\}, \\ M_2 &:= \Big\{x = (x_1, x_2, x_3) \in \mathbb{R}^3_h : h_1 < x_3 < h_2\Big\}, \\ M_3 &:= \Big\{x = (x_1, x_2, x_3) \in \mathbb{R}^3_h : h_2 < x_3 < h\Big\}, \end{aligned}$$

where h_1 and h_2 are positive constants.

Review. As we known that the submerged acoustic model is subject to transmission loss due to the absorption of acoustic energy by the geometric spreading and the propagation medium. And the sound waves may have refractions and reflections not only at the ocean surface Γ_+ and the seabed Γ_- but also at the interface $\Gamma_i\,(i = 1, 2)$ of the adjacent layers. Moreover, the refractive index $n(x)$ and the sound velocity $c(x)$ are depending mainly on the depth of ocean [26], and the waves scattered by a compact object or a local inhomogeneity in a stratified waveguide may not satisfy the well-known Sommerfeld radiation condition which is the fundamental assumption of scattering theory in a homogeneous medium. All these typical features indicate that the scattering problems in the stratified waveguide are much more difficult and complex than the ones in the one-layered waveguide. Nevertheless, Prof. Gilbert, Prof. Xu and coauthors also have obtained lots of impressive results for the scattering problems of the stratified waveguide, for example, the generalized Sommerfeld radiation condition and the Green's function [28, 33], the well-posedness analysis and the uniqueness analysis [6, 30, 32], the numerical methods and analysis for the scattered fields [6, 10, 15, 29], the efficient reconstruction methods for sources and scatterers[11, 19, 31, 32] and references therein. In addition, Prof. Xu, Prof. Liu and coauthors focus on the model of the three-layered waveguide and propose some effective direct methods (DM) for identifying marine sources and scatterers [22, 23, 24, 25, 26]. The DM rely on some index functions which help to provide a "gap" between the interior and the exterior of inhomogeneities, thus the locations and shapes of inhomogeneities can be recovered efficiently. In addition, the DM only apply some simple calculations, and don't involve any matrix inversions or solutions of large-scale ill-posed linear systems or optimization procedures, so they exhibit several impressive strengths: immediate, highly tolerant to noise, fast, simple and easy to carry out.

Main contribution. In this paper, we concern with the simultaneous detection of the sources and scatterers from the far-field data in a *three-dimensional stratified ocean waveguide* $\mathbb{R}^3_h$. Assume a time harmonic point source located at $x^s := (\bar{x}^s, x^s_3) \in \mathbb{R}^3_h$ and an inhomogeneous scatterer Ω with any geometrical shape is compactly contained in the waveguide, and the other part of the stratified waveguide is connected. Moreover, the scatterer Ω could be the wave-penetrable inclusion or the wave-impenetrable object. Without loss of generality, we suppose Ω is situated in the thermocline M_2, and the configuration is shown in Figure 2(b). Due to the presence of the sources and the obstacles, the total acoustic pressure field u without convection satisfies the outgoing radiation condition [22] and the following Helmholtz equation:

$$\Delta u + k^2(x_3)n^2(x)u = -\delta(x - x^s), \quad x \in \mathbb{R}^3_h, \tag{1.3}$$

where $k(x_3)$ stands for the wavenumber which depends basically on the depth of ocean, and $n(x)$ means the refractive index. To the best of the authors' knowledge, the simultaneous reconstruction of marine sources and scatterers in the three-dimensional stratified ocean waveguide are rarely investigated and addressed in the literature. Accordingly, we shall extend the direct method in [26] to identify the marine sources and scatterers simultaneously from the far-field pattern u_∞, where u_∞ is induced from the total acoustic field u. The extended direct method (EDM) is computationally quite cheap and work with very few incidences and receivers, and the numerical simulations indicate that it can provide good and reasonable estimations for the embedded sources and scatterers, even in the presence of a large amount of noise in the measured data. Moreover, the EDM does not need a priori information such as the number of disconnected components or the physical features of the embedded inhomogeneities. Consequently, the EDM can naturally serve as simple and efficient algorithm for providing reliable initial guesses of the embedded

inhomogeneities for any existing more refined but computationally more demanding methods to identify the true physical profiles (i.e. refractive index, shape, magnetic permeability and density). Considering the severe ill-posedness of inverse scattering problems in the stratified ocean waveguide, the appropriate and reliable initial sampling regions for the embedded inhomogeneities may save a fundamental part of computational efforts in the entire reconstruction procedure.

Outline of the paper. The remainder of this paper is organized as follows. In Section 2, we shall state the direct scattering problem in the stratified ocean waveguide. Section 3 presents an extended direct method for imaging the marine sources and scatterers simultaneously in the stratified ocean waveguide, which is efficient, robust against noise and ease of implementation. In Section 4, we shall carry out some numerical experiments to evaluate the performance of the EDM in the marine detections. Finally, some concluding remarks are exhibited in Section 5.

2 The direct scattering problem

In this section, we describe the direct scattering problem in the three-dimensional stratified ocean waveguide $\mathbb{R}^3_h$.

Modeling the direct scattering problem. Suppose that both the sources x^s and the scatterers Ω are contained in the stratified ocean waveguide $\mathbb{R}^3_h$ and needed to be identified. The total acoustic pressure field u without convection satisfies the outgoing radiation condition [22], the boundary conditions (1.1) and (1.2), and the Helmholtz equation (1.3). We can rewrite them compactly as follows:

$$\begin{cases} \Delta u + k^2(x_3)n^2(x)u = -\delta(x - x^s), \quad x \in \mathbb{R}^3_h, \\ u = 0 \ \text{ on } \ \Gamma_+, \quad \frac{\partial u}{\partial \nu} = 0 \ \text{ on } \ \Gamma_-, \\ \rho_+ u_+ = \rho_- u_-, \quad \frac{\partial u_+}{\partial \nu} = \frac{\partial u_-}{\partial \nu} \ \text{ on } \ \Gamma_i \, (i = 1, 2). \end{cases} \tag{2.1}$$

In addition, for the *penetrable* scatterer Ω, u also satisfies the following continuous conditions, namely,

$$\rho_+ u_+ = \rho_- u_- \quad \text{and} \quad \frac{\partial u_+}{\partial \nu} = \frac{\partial u_-}{\partial \nu} \quad \text{on} \quad \partial\Omega, \tag{2.2}$$

where ν is the normal vector, and subscripts $+$ and $-$ represent the variable x approaching the boundary $\partial\Omega$ from the interior and the exterior of scatterer respectively. Assume the scatterer Ω is *impenetrable*, which possesses the sound-soft boundary condition (also known as the Dirichlet boundary condition), the total acoustic field u satisfies

$$u = 0 \ \text{ on } \ \partial\Omega. \tag{2.3}$$

Methodology for the direct scattering problem. Suppose the density between the penetrable scatterer Ω and the thermocline M_2 (the layer contains Ω) is small, the total acoustic field u satisfies (2.1) and (2.2), which can be expressed as [22, 25]

$$u(x; x^s) = G(x; x^s) + \int_\Omega \tau(y)\, G(x; y) u(x^s; y) dy, \quad x \in \mathbb{R}^3_h, \tag{2.4}$$

where $G(x; x^s)$ means the Green's function, $\tau(y) = k^2_\Omega n_\Omega(y)^2 - k^2(y_3)n^2(y_3)$ for the interior of the medium obstacle Ω and $\tau = 0$ for the other areas, k_Ω and $n_\Omega(y)$ stand for the wavenumber and the refractive index of the object respectively. Considering the scatterer Ω is sound-soft, the total acoustic field u satisfies (2.1) and (2.3), which has the following representation [28]:

$$u(x; x^s) = G(x; x^s) + \int_{\partial\Omega} \left\{ u(x^s; y) \frac{\partial G(x; y)}{\partial \nu} - G(x; y) \frac{\partial u(x^s; y)}{\partial \nu} \right\} dS(y), \quad x \in \mathbb{R}^3_h \backslash \overline{\Omega}. \tag{2.5}$$

The Green's function $G(x; x^s)$ in (2.4) and (2.5) has the following Hankel transform expression [22, 26]:

$$G(x; x^s) = -\frac{1}{2\pi} \int_0^\infty \frac{\varphi_1(\xi, x_3^{max}) \varphi_2(\xi, x_3^{min})}{W(\varphi_1, \varphi_2)} J_0(\xi r) \xi d\xi \,, \tag{2.6}$$

where $r = |\bar{x} - \bar{x}^s|$, $x_3^{max} = \max\{x_3, x_3^s\}$, $x_3^{min} = \min\{x_3, x_3^s\}$, φ_1 and φ_2 are the modes of the propagating waves, $J_0(\xi r) = \sum_{m=0}^{\infty} \frac{(-1)^m}{(m!)^2} \left(\frac{\xi^2 r^2}{4}\right)^m$ is the zero-order Bessel function of the first kind, and W denotes the Wronskian which is

$$W(\varphi_1, \varphi_2) = \begin{vmatrix} \varphi_1 & \varphi_2 \\ \varphi_1' & \varphi_2' \end{vmatrix}.$$

It is worth mentioning that the Hankel transform representation (2.6) is widely applicable at intermediate distances, and it can be transformed into the normal mode representation with the help of the residual evaluation [6, 32]. Because the Wronskian $W(\varphi_1, \varphi_2)$ has a finite number of zeros, we can rewrite the expression (2.6) into the following form by employing the contour integration of the complex plane and the residual theorem [22, 26]:

$$G(x; x^s) = -\frac{i}{2} \sum_{n=0}^{\infty} \frac{\varphi_1(\xi_n, x_3^{max}) \varphi_2(\xi_n, x_3^{min})}{W'(\varphi_1, \varphi_2)} H_0^{(1)}(\xi_n r), \tag{2.7}$$

where ξ_n stands for the zeros of the Wronskian $W(\varphi_1, \varphi_2)$. The behavior of the Green's function can be found in [22], and the far-field behavior of the Green's function is presented in [26]. We would like to remark that the Green's function also has the multiple scattering representation and the normal mode expression. When the receiving point is far away from the sound source, the normal mode representation is rather useful since it exhibits the behaviors of the propagating modes. And the multiple scattering representation shows the behaviors of the incidences and the first few reflective and refractive waves, so it is quite helpful at distances which are close to the sound source. These three expressions of Green's function can be transformed into each other under appropriate operations, we refer the readers to [3, 6] for the details.

Based on (2.4), the corresponding far-field pattern takes the form

$$u_\infty(x^r; x^s) = G_\infty(x^r; x^s) + \int_\Omega \tau(y) u(x^s; y)\, G_\infty(x^r; y) dy, \tag{2.8}$$

where $x^r = (\bar{x}^r, x_3^r)$ with $\bar{x}^r$ belongs to the unit circle $\mathbb{S}$, and $G_\infty(x; x^s)$ is represented as

$$G_\infty(x^r; y) = \sum_{n=1}^{\infty} \varphi_1^n(x_3^r) \varphi_1^n(x_3) e^{-i\xi_n \bar{x}^r \cdot \bar{y}},$$

where $\varphi_1^n(x_3^r)$ is short for $\varphi_1(\xi_n, x_3^r)$ and $\varphi_1^n(\cdot) = i c_n \varphi_2^n(\cdot)$ for some constant c_n. The far-field pattern for (2.5) is

$$u_\infty(x^r; x^s) = G_\infty(x^r; x^s) + \int_{\partial\Omega} \left\{ u(x^s; y) \frac{\partial G_\infty(x^r; y)}{\partial \nu} - G_\infty(x^r; y) \frac{\partial u(x^s; y)}{\partial \nu} \right\} dS(y). \tag{2.9}$$

In the practical applications, the Green's function is truncated into a finite summation, and the direct problem is the calculation of the far-field pattern (2.8) or (2.9) with the source(s) x^s and the receiver(s) x^r, we refer to [6, 22, 26, 32] for the numerical approaches.

3 The extended direct method for the inverse scattering problem

In this section, we shall propose an *extended direct method* (EDM) for the inverse scattering problem in the three-dimensional stratified ocean waveguide $\mathbb{R}_h^3$.

The main target of the EDM is to construct indicator functions which have fairly different behaviors inside and outside of the inhomogeneities, therefore the inhomogeneities can be identified simultaneously by the effective index functions. Now we state the inverse scattering problem of our interest in the following first subsection.

3.1 The inverse scattering problem

In this subsection, we shall describe the inverse scattering problem of our interest in the three-dimensional stratified ocean waveguide.

Reformulation of the inverse scattering problem. Suppose that the marine sources x^s and scatterers Ω are unknown and embedded in a sampling region D, and the receivers x^r are situated at the following cylindrical surface Γ_c:

$$\Gamma_c = \left\{ x = (x_1, x_2, x_3) := (\bar{x}, x_3) \in \mathbb{R}^3_h \Big| |\bar{x}| = 1, x_3 \in [0, h] \right\},$$

where Γ_c is centered at x_3-axis.

We first concern with a medium scatterer Ω with the continuous conditions (2.2), and the domain of the scatterer is discretized into a set of tiny cubes, where the volume of each element is denoted as $\sigma_p \, (p = 1, 2, \cdots, N)$ respectively. With the rectangular quadrature, the far-field pattern (2.8) is approximated as

$$u_\infty(x^r; x^s) \approx G_\infty(x^r; x^s) + \sum_{p=1}^{N} \sigma_p \tau(y^p) u(x^s; y^p) G_\infty(x^r; y^p), \quad x^r \in \Gamma_c, \ x^s \in D, \tag{3.1}$$

where y^p is the coordinate of the p-th element.

We then consider an impenetrable obstacle Ω with the sound-soft boundary condition (2.3). Likewise, the far-field pattern (2.9) can be estimated as

$$u_\infty(x^r; x^s) \approx G_\infty(x^r; x^s) - \sum_{p=1}^{N} \tilde{\sigma}_p \frac{\partial u(x^s; y^p)}{\partial \nu} G_\infty(x^r; y^p), \quad x^r \in \Gamma_c, \ x^s \in D, \tag{3.2}$$

where the boundary $\partial\Omega$ is divided into a set of small elements and $\tilde{\sigma}_p \, (p = 1, 2, \cdots, N)$ means the area of each element, y^p stands for the coordinate of the p-th element.

As the sources x^r and the obstacles Ω are unknown in advance, **the inverse scattering problem of our interest is reformulated as follows:**

identify the geometrical profiles (e.g., locations, shapes and sizes) of them from the far-field pattern $u_\infty(x^r; x^s)$.

We would like to remark that the uniqueness analysis had been studied by Prof. Gilbert, Prof. Xu and coauthors in the references [6, 32].

3.2 The extended direct method

In this subsection, the extended direct method (EDM) would be proposed for the simultaneous detection of the embedded sources and scatterers in the three-dimensional stratified ocean waveguide.

Derivation of EDM. We first recall the orthogonality of the modes $\varphi_1^n(x_3)$ [6, 22, 32]:

$$\int_0^h \varphi_1^n(x_3) \varphi_1^m(x_3) dx_3 = \begin{cases} C & \text{for} \quad m = n, \\ 0 & \text{for} \quad m \neq n, \end{cases} \tag{3.3}$$

where C is a nonzero constant. With the orthogonality (3.3) and the Graf's addition theorem, the inner product of $G_\infty(x^r; x)$ and $\overline{G}_\infty(x^r; x^q)$ over the cylindrical surface Γ_c with respect to x^r can be simplified as follows:

$$
\begin{aligned}
&\int_{\Gamma_c} G_\infty(x^r;x)\overline{G}_\infty(x^r;x^q)dS(x^r)\\
&=\int_{\mathbb{S}}\int_0^h \sum_{n=1}^{\infty}\varphi_1^n(x_3^r)\varphi_1^n(x_3)e^{-i\xi_n\bar{x}^r\cdot\bar{x}}\sum_{m=1}^{\infty}\varphi_1^m(x_3^r)\varphi_1^m(x_3^q)e^{i\xi_m\bar{x}^r\cdot\bar{x}^q}dx_3^r\,d\bar{x}^r\\
&=C\sum_{n=1}^{\infty}\varphi_1^n(x_3)\varphi_1^n(x_3^q)\int_{\mathbb{S}}e^{i\xi_n\bar{x}^r(\bar{x}^q-\bar{x})}d\bar{x}^r\\
&=2\pi C\sum_{n=1}^{\infty}\varphi_1^n(x_3)\varphi_1^n(x_3^q)J_0(\xi_n|\bar{x}^q-\bar{x}|),
\end{aligned}
\tag{3.4}
$$

where $x, x^q \in D$, J_0 is the zero-order Bessel function of the first kind.

Considering the scatterer Ω is penetrable, and the far-field pattern is estimated by (3.1). Multiplying (3.1) by the conjugate of $G_\infty(x^r;x^q)$ with x^q belongs to the sampling region D, and take the integral over the cylindrical surface Γ_c with respect to x^r, the following derivation is obtained with the aid of (3.4):

$$
\int_{\Gamma_c} u_\infty(x^r;x^s)\overline{G}_\infty(x^r;x^q)dS(x^r) \tag{3.5}
$$

$$
= \int_{\Gamma_c} G_\infty(x^r;x^s)\overline{G}_\infty(x^r;x^q)dS(x^r)+\sum_{p=1}^{N}\sigma_p\tau(y^p)u(x^s;y^p)\int_{\Gamma_c} G_\infty(x^r;y^p)\overline{G}_\infty(x^r;x^q)dS(x^r)
$$

$$
= 2\pi C\Big[\widetilde{G}(x^s;x^q)+\sum_{p=1}^{N}\sigma_p\tau(y^p)u(x^s;y^p)\widetilde{G}(y^p;x^q)\Big], \tag{3.6}
$$

where $\widetilde{G}\big((\cdot);x^q\big) = \sum_{n=1}^{\infty}\varphi_1^n\big((\cdot)_3\big)\varphi_1^n(x_3^q)J_0\big(\xi_n r\big)$ with $r = |\bar{x}^q - \bar{(\cdot)}|$. Based on the singular manner of Bessel function $J_0(r)$ (see Figure 3), $\widetilde{G}\big((\cdot);x^q\big)$ becomes relatively large as x^q moves close to the inhomogeneities x^s and x^p, and it decays rapidly when x^q moves away from them. This distinct property can be applied in the reconstruction process by the inner product (3.5).

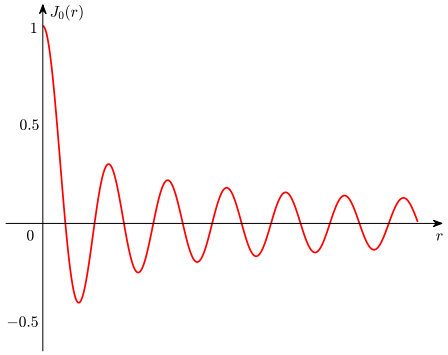

Figure 3: *The demonstration of the Bessel function* $J_0(r)$.

Now we concern with the sound-soft obstacle Ω, and the far-field pattern is approximated by (3.2). Likewise, we multiply (3.2) by $\overline{G}_\infty(x^r;x^q)$, and take the integral over the cylindrical surface Γ_c with

respect to x^r, the following derivation can be acquired with the aid of (3.4):

$$\int_{\Gamma_c} u_\infty(x^r;x^s)\overline{G}_\infty(x^r;x^q)dS(x^r) \tag{3.7}$$

$$= \int_{\Gamma_c} G_\infty(x^r;x^s)\overline{G}_\infty(x^r;x^q)dS(x^r) - \sum_{p=1}^{N}\tilde{\sigma}_p\frac{\partial u(x^s;y^p)}{\partial\nu}\int_{\Gamma_c} G_\infty(x^r;y^p)\overline{G}_\infty(x^r;x^q)dS(x^r)$$

$$= 2\pi C\left[\widetilde{G}(x^s;x^q) - \sum_{p=1}^{N}\tilde{\sigma}_p\frac{\partial u(x^s;y^p)}{\partial\nu}\widetilde{G}(y^p;x^q)\right], \tag{3.8}$$

where x^q expresses any point in the sampling domain D. We can observe that the singular manner of $\widetilde{G}\big((\cdot);x^q\big)$ can serve as the crucial ingredient in identifying the unknown inhomogeneities by the inner product (3.7).

Now we are ready to propose the first indicator function:

$$I_1(x^q) = \big|\langle u_\infty(x^r;x^s), G_\infty(x^r;x^q)\rangle_{L^2(\Gamma_c)}\big| \quad \text{for} \quad x^q \in D, \tag{3.9}$$

where the L^2-inner product is defined in (3.5) or (3.7). In order to obtain accurate and reliable reconstructions of the inhomogeneities, the volume of each cube σ_p in (3.6) and the area of each cube $\tilde{\sigma}_p$ in (3.8) usually take extremely small values in the practical applications, for instance, $\sigma_p = 1.25\times10^{-4}$ and $\tilde{\sigma}_p = 2.5\times10^{-3}$ when the length of cube is selected as 0.05. As shown in Figure 3, the Bessel function $J_0(r)$ possesses the maximum value 1. Consequently, the first terms in (3.6) and (3.8) are the dominant parts which means the index function $I_1(x^q)$ in (3.9) can only indicate the locations of the embedded sources. For the purpose of identifying the scatterers, we define another index function as follows:

$$I_2(x^q) = \big|\langle u_\infty(x^r;x^s) - G_\infty(x^r;x^s), G_\infty(x^r;x^q)\rangle_{L^2(\Gamma_c)}\big| \quad \text{for} \quad x^q \in D\backslash\{x^s\}, \tag{3.10}$$

where the source locations x^s are already acquired from $I_1(x^q)$. Owing to the dominant terms in (3.6) and (3.8) are eliminated, the indicator function $I_2(x^q)$ can provide the positions of the embedded marine scatterers Ω.

We would like to state some remarks for the index functions: the function $\overline{G}_\infty(x^r;x^q)$ in the indicators (3.9) and (3.10) can be replaced by $\sum_{m=1}^{\infty}\varphi_1^m(x_3^r)e^{i\xi_m\bar{x}^r\cdot\bar{x}^q}$, and the corresponding function $\widetilde{G}\big((\cdot);x^q\big)$ would be replaced by $\sum_{n=1}^{\infty}\varphi_1^n\big((\cdot)_3\big)J_0\big(\xi_n r\big)$ which also possesses the singular property; the indicator function $I_i(x^q)$ $(i=1,2)$ is normalized in the practical applications; the value of index function $I_i(x^q)$ $(i=1,2)$ is selected as the maximum for the multiple data sets.

Numerical implmentation of EDM. The extended direct method (EDM) is carried out by the following steps:

1. Choose a sampling region D that contains the unknown inhomogeneities, and select a fine mesh on D. Choose a cut-off value ϱ.

2. Calculate the value of index function $I_1(x^q)$ for each sampling point $x^q \in D$ by (3.9), and eliminate x^q when $I_1(x^q) < \varrho$. Output all the grid points in D as the estimate of the source(s), and these points are denoted as x^s.

3. Compute the value of indicator function $I_2(x^q)$ for each sampling point $x^q \in D\backslash\{x^s\}$ by (3.10), and drop x^q when $I_2(x^q) < \varrho$. Output all the grid points in $D\backslash\{x^s\}$ as the approximation of the scatterer(s).

4. Combine the remaining points in Step 2 with the ones in Step 3, and they are the reconstructions of the unknown inhomogeneities.

It is worth mentioning two special cases for applying EDM during the reconstruction procedures: if no grid point is output in the Step 3 of EDM, the sampling domain D may only contain the marine source(s) and the algorithm can be terminated; if all the gird points are eliminated in the Step 2 of EDM which may indicate no source point is embedded in the sampling region D, we can stop the algorithm and bring in some incidences and employ the direct method in [26] for the identifications of the marine scatterers.

4 Numerical simulations

In this section, some numerical examples are exhibited to evaluate the robustness and effectiveness of the extended direct method (EDM) by employing the far-field pattern for recovering marine sources and scatterers simultaneously in the three-dimensional stratified ocean waveguide $\mathbb{R}^3_h$.

Setup of numerical experiments. Initially, we introduce the numerical settings that are applied in the following simualtions. The heights of the waveguide are selected as $h_1 = 100/3$, $h_2 = 200/3$ and $h = 100$, respectively. In each layer $M_i (i = 1, 2, 3)$, the wavenumber is set to be $k_i = 2\pi f/c_i$, where the velocities are respectively chosen as $c_1 = 1800, c_2 = 1200$ and $c_3 = 1600$, and the frequency f is 75. Moreover, the refractive indices in each layer are separately set to be $n_1 = 1.5, n_2 = 3$ and $n_3 = 2$, and the corresponding densities are selected as $\rho_1 = 1500, \rho_2 = 1200$ and $\rho_3 = 1000$ respectively. The density of the scatterer is set as 1100.

We solve the equation $W(\varphi_1, \varphi_2)(\xi) = 0$ to derive all the positive roots and a few negative zeros ξ_n (the negative zeros are greater than -40) for the evaluation of $G_\infty(x^r, \cdot)$ numerically. The mesh size of the forward problem is taken to be 0.02 while the one for the inverse problem is selected as 0.09. The far-field pattern are computed numerically from (3.1) and (3.2) with $x^s \in D$ and $x^r \in \Gamma_c$. The demonstration of the numerical settings are shown in Figure 4, where the cyan pentagram represents the receivers, the tiny red diamond means the sources and the greenyellow ellipsoids are the scatterers. Moreover, the noisy data is generated as follows:

$$u^\delta_\infty(x^r; x^s) = u_\infty(x^r; x^s)\left[1 + \delta \frac{\ell_1(x^r) + i\,\ell_2(x^r)}{\|\ell_1(x^r) + i\,\ell_2(x^r)\|}\right] \quad \text{for } x^r \in \Gamma_c,$$

where δ means the noise level which is usually selected as 10% unless specified otherwise, ℓ_1 and ℓ_2 stand for two random numbers varying from -1 to 1. It is worth mentioning that when calculating the far-field pattern of the forward problem, we have made the numerical results as accurate as our computer can, and the remaining error would serve as the extra noise in the inverse problem.

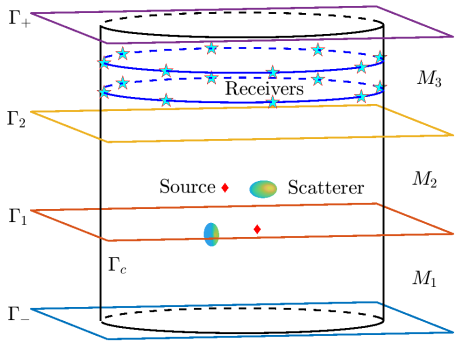

Figure 4: *The demonstration of the numerical settings.*

The contrast function τ of the medium obstacle is set to be 1 in the following experiments unless specified otherwise, and the indicator functions $I_1(x^q)$ and $I_2(x^q)$ are normalized so that their maximums are 1. In the following numerical experiments, the sampling point with the value of index function larger

than the cut-off value ϱ would be regarded as the inhomogeneities while the others are dropped as the area of the stratified ocean waveguide. The cut-off value ϱ is usually taken as 0.9 in the following numerical simulations unless specified otherwise. Moreover, we consider the center point of the reconstruction of marine source as the recovered source location.

Experiment 1. We concern with two medium inclusions in the diagonal position, which take up the following two regions:

$$\Omega_1 = [41, 42] \times [48, 49] \times [62, 63], \quad \Omega_2 = [48, 49] \times [41, 42] \times [68, 69],$$

which are separately located in the thermocline M_2 and the surface layer M_3, see the cyan cubes in Figure 5(a). The sampling domain D is selected as

$$D = [38, 52] \times [38, 52] \times [58, 72],$$

see the black box in Figure 5(a). Three point sources are contained in D, which are situated at $(42, 42, 62)$, $(45, 45, 66)$ and $(47, 48, 68)$ respectively, see the red rhombic points in Figure 5(a). We can observe that the volume of D is around 2700 times greater than the volume of each object. Only 16 observation angles $(\cos(n\pi/4), \sin(n\pi/4), 60 + 15m)$ $(n = 1, 2, \cdots, 8, m = 0, 1)$ are employed in the identification.

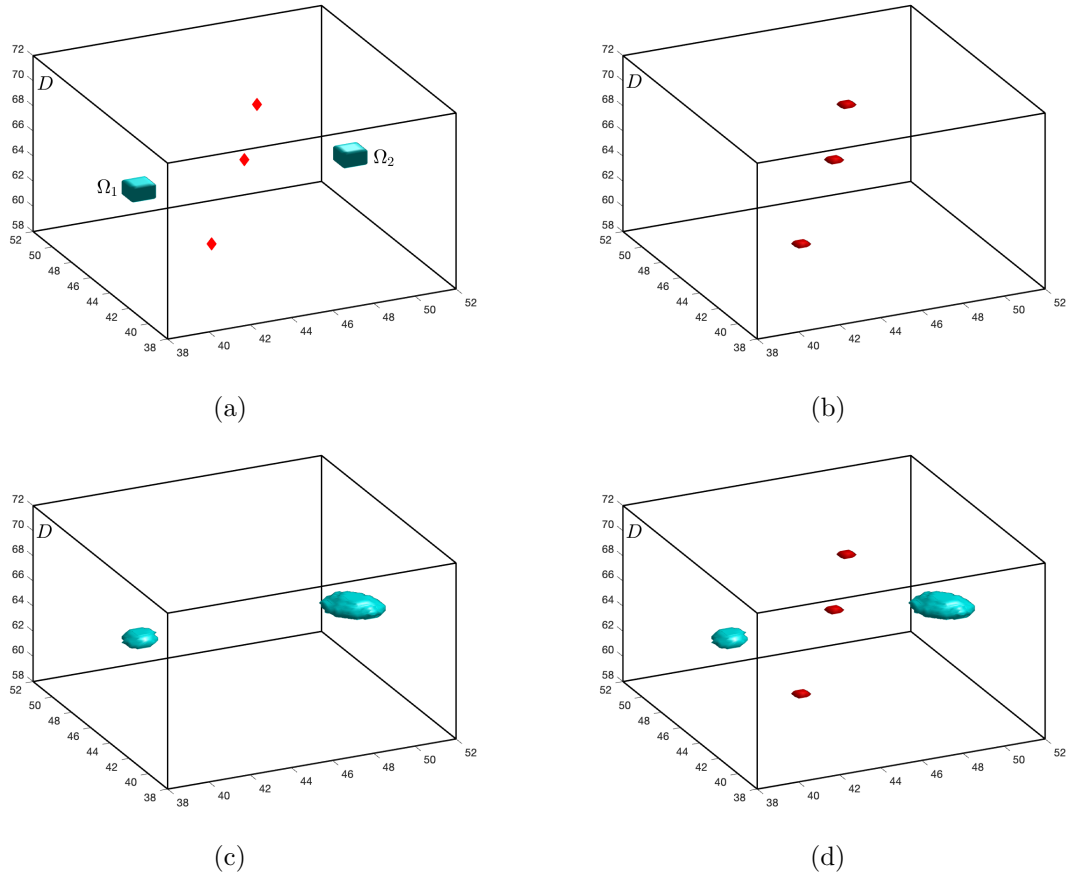

Figure 5: *For the Experiment 1, (a) the true inhomogeneities, (b) the recoveries of sources, (c) the reconstructions of scatterers and (d) the identifications of inhomogeneities.*

For the presence of 10% random noise, the recovery of the sources are shown in Figure 5(b) while the reconstruction of the medium scatterers are presented in Figure 5(c), and the combination of them are exhibited in Figures 5(d). Considering the fact that only 3 sources and very few observation data are applied in the reconstruction process, the identifications of inhomogeneities are reliable and reasonable.

We can conclude that the EDM is capable of identifying the inhomogeneities in different layers even if the measured data are perturbed.

Experiment 2. This example investigates two impenetrable objects with the Dirichlet conditions, which are located closely in the parallel positions:

$$\Omega_1 = [42, 43] \times [48, 49] \times [62, 63], \quad \Omega_2 = [47, 48] \times [48, 49] \times [62, 63].$$

Both of them are situated in the thermocline M_2, see the cyan cubes in Figure 6(a). The sampling region D is also taken as

$$D = [38, 52] \times [38, 52] \times [58, 72],$$

see the black box in Figure 6(a). The sampling domain D contains three sources, which are placed at $(42, 45, 65)$, $(45, 43, 62)$ and $(48, 42, 66)$ respectively, see the red rhombic points in Figure 6(a). Likewise, the volume of D is around 2700 times greater than the volume of each obstacle. We apply 24 observation angles $(\cos(n\pi/4), \sin(n\pi/4), 60 + 15m)$ $(n = 1, 2, \cdots, 8, m = 0, 1, 2)$ in the reconstruction procedure.

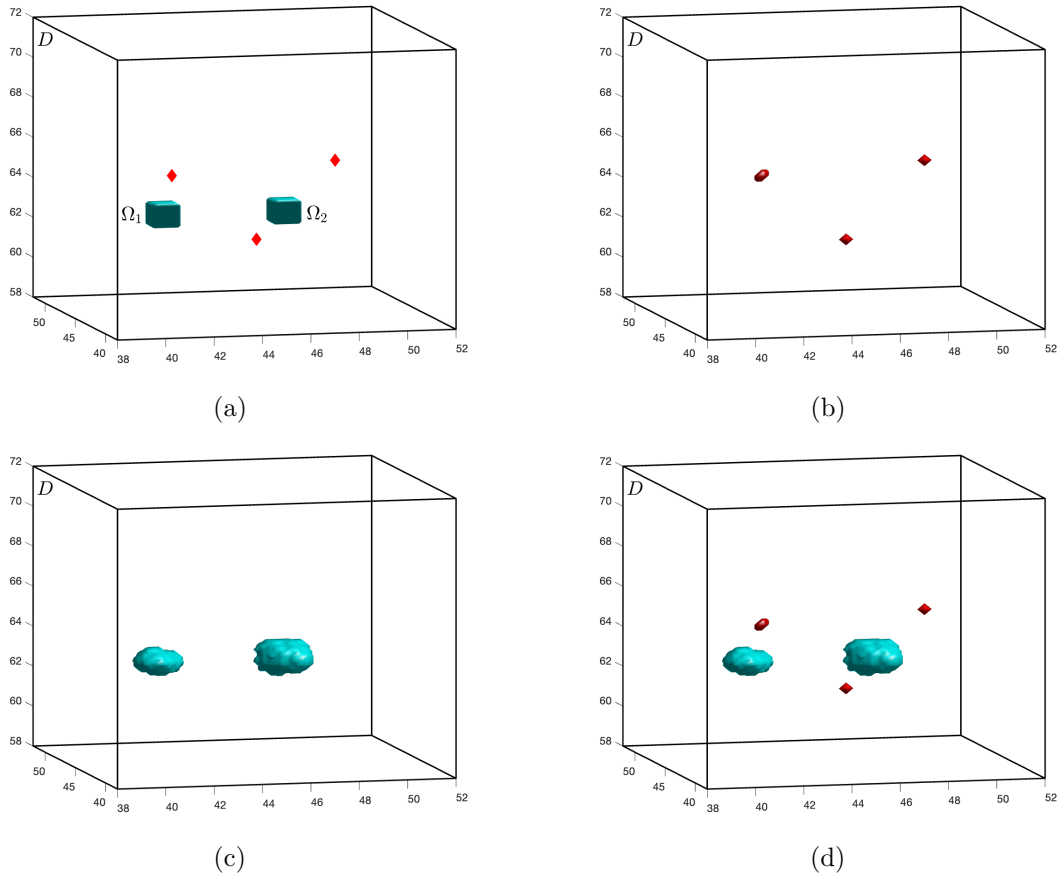

Figure 6: *For the Experiment 2, (a) the true inhomogeneities, (b) the recoveries of sources, (c) the reconstructions of scatterers and (d) the identifications of inhomogeneities.*

The recoveries of the sources and the scatterers under 10% random noise are respectively shown in Figures 6(b) and (c). The approximations of inhomogeneities in Figure 6(d) are impressive and reliable since the reconstructions agree well with the true ones, and the two closely situated impenetrable objects are clearly separated.

Experiment 3. We consider a L-shaped medium inclusion in this experiment, which occupies the following locations:

$$[44, 47] \times [46, 47] \times [63, 64] \quad \text{and} \quad [43, 44] \times [46, 47] \times [64, 68],$$

see the cyan L-shaped rod in Figure 7(a). The same sampling domain D as in Experiment 2 is laid out, and four marine sources with the locations $(42, 49, 67)$, $(45, 43, 63)$, $(49, 46, 62)$ and $(45, 49, 67)$ are embedded in the sampling region, see the black box and the red rhombic points in Figure 7(a) for demonstration. We employ 48 observation angles $(\cos(n\pi/8), \sin(n\pi/8), 45 + 15m)$ $(n = 1, 2, \cdots, 16, m = 0, 1, 2)$ in the reconstruction procedure.

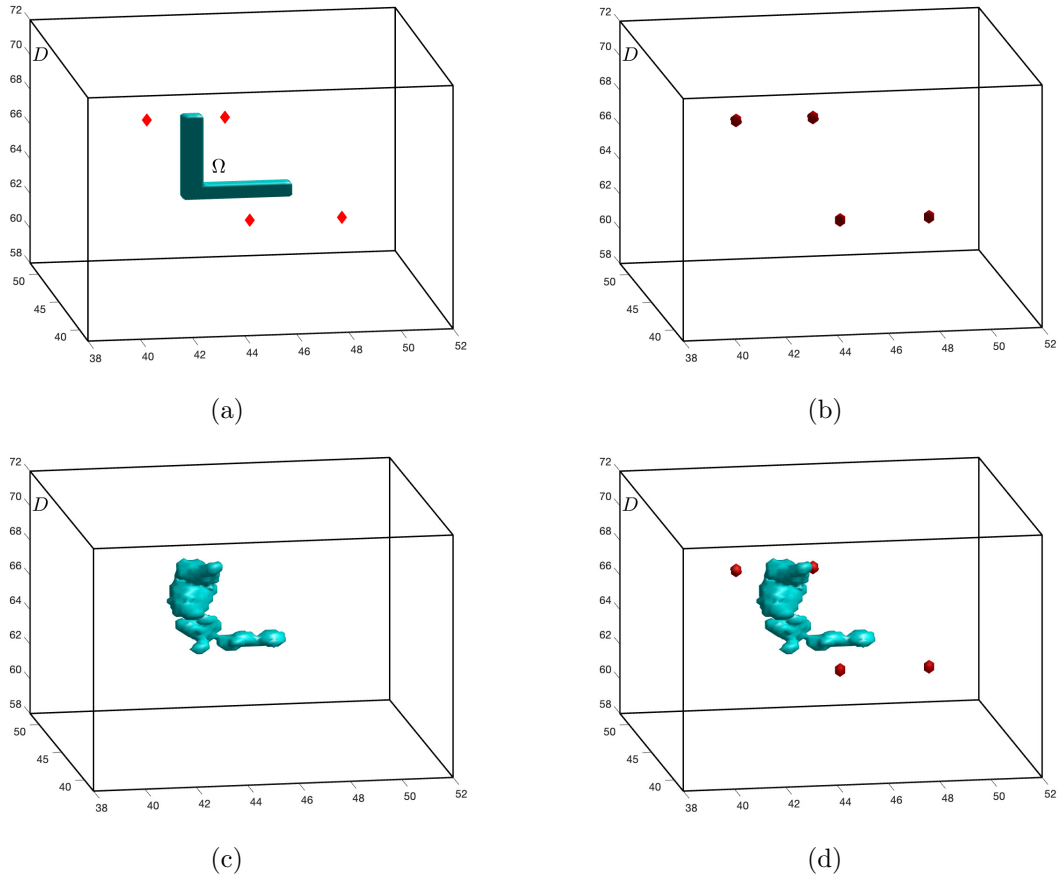

Figure 7: *For the Experiment 3, (a) the true obstacle, (b) the recoveries of sources, (c) the reconstruction of scatterer and (d) the identifications of inhomogeneities.*

The identifications of the sources and the scatterer under 10% random noise are respectively shown in Figures 7(b) and (c). Considering only four sources are used in the reconstruction process, the reconstructions of inhomogeneities in Figure 7(d) are reasonable and acceptable. In addition, if we apply some more incidences with the directions $(\cos((2j-1)\pi/4), \sin((2j-1)\pi/4), 45+15m)$ $(j = 1, 2, 3, m = 0, 1, 2)$ to detect the L-shaped obstacle in the third step of EDM, the recovery is much better and exhibited in Figure 8. Therefore, we suggest employing some more incidences in the third step of EDM for identifying the marine scatterers.

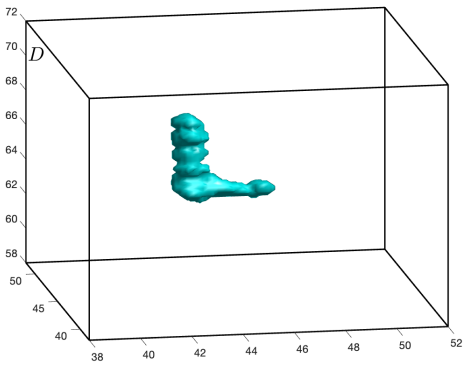

Figure 8: *The reconstruction of the L-shaped scatterer in Experiment 3.*

Finally, we can conclude that the EDM is dependable and applicable to reconstruct the inhomogeneities simultaneously in the stratified ocean waveguide, and it can serve as an effective approach for supplying the initial guesses of marine inhomogeneities for any existing more advanced and refined but computationally more demanding methods to identify the true physical profiles.

5 Conclusions

In this paper, we extend the direct imaging method in [26] for simultaneously identifying embedded sources and scatterers in a stratified ocean waveguide $\mathbb{R}^3_h$. The advantages of the EDM can be concluded as follows:

(1). The proposed extended direct method (EDM) only employ the simple inner product operation, without any matrix inversions, nonlinear optimizations or solution procedures involved, so it is ease of implementation and computationally quite cheap.

(2). The robustness and effectiveness of the EDM in the reconstruction procedure has been shown via numerical simulations.

(3). The EDM can not only identify the sources in different locations but also can reconstruct the scatterers in different shapes (i.e. cubes and L-shaped object) and positions (i.e. closely situated obstacles) in the practical applications. Since the proposed algorithm is simple, fast and highly tolerant to noise, it can be considered as an efficient numerical approach for providing reliable estimations of the marine inhomogeneities in the true ocean environment.

Considering the severe ill-posedness of inverse scattering problems in the marine acoustics, the decrease of the sizes of initial sampling regions for the embedded marine inhomogeneities may fundamentally release the computational burden in the entire reconstruction process. In addition, simultaneous reconstruction of the marine sources and obstacles from the near-field data in the three-dimensional stratified ocean waveguide is a promising topic. Above mentioned issues need further discussing in the near future.

Acknowledgement

The work of Keji Liu was supported by the NNSF of China under grant No. 12071275, the Science and Technology Commission of Shanghai Municipality under grant No. 20ZR1418800. The work of Dinghua Xu was supported by the NNSF of China under grant No.11871435 and No.91534113.

References

[1] H. Ammari, E. Iakovleva and H. Kang, *Reconstruction of a small inclusion in a 2D open waveguide*, SIAM J. Appl. Math. **65** 2107-2127, 2005.

[2] H. Ammari, E. O. Hiltunen and S. Yu, *Subwavelength guided modes for acoustic waves in bubbly crystals with a line defect*, J. Eur. Math. Soc., 2021, DOI: 10.4171/JEMS/1126.

[3] D. Ahluwalia and J. Keller, *Exact and asymptotic representations of the sound field in a stratified ocean*, in Wave Propagation and Underwater Acoustics, Lecture Notes in Phys. **70**, Springer, Berlin 14-85, 1977.

[4] J. Buchanan and R. Gilbert, *Determination of the coefficients of an elastic seabed*, Appl. Anal. **68** 75–86, 1998.

[5] J. Buchanan, R. Gilbert and A. Wirgin, *Finding an inclusion in a shallow ocean using the ICBA method*, Appl. Anal. **71** 347–378, 1999.

[6] J. Buchanan, R. Gilbert, A. Wirgin and Y. Xu, *Marine acoustics: Direct and inverse problems*, SIAM, Philadelphia, 2004.

[7] J. Buchanan, R. Gilbert and Y. Xu, *Green's function representation for acoustic pressure over a poroelastic seabed*, Appl. Anal. **65** 57–68, 1997.

[8] R. Gilbert, *Biography of Robert Pertsch Gilbert*, Comp. Vari. Ellip. Equ. **57** 113-120, 2012.

[9] R. Gilbert and W. Lin, *Wavelet solutions for time harmonic acoustic waves in a finite ocean*, J. Comput. Acoust. **1** 31–60, 1993.

[10] R. Gilbert and W. Lin, *Acoustic field in a shallow, stratified ocean with a poroelastic seabed*, Z. Angew. Math. Mech. **77** 677–688,1997.

[11] R. Gilbert, C. Mawata and Y. Xu, *Determination of a distributed inhomogeneity in a two-layered waveguide from scattered sound*, Dir. Inv. Probl. Math. Phys. **5** 107–124, 2000.

[12] R. Gilbert, Y. Xu, D. Wood, *Construction of approximations to acoustic Green's functions for nonhomogeneous oceans using transmutation*, Wave Motion **10** 285–297, 1988.

[13] R. Gilbert, Y. Xu, *Dense sets and the projection theorem for acoustic waves in a homogeneous finite depth ocean*, Math. Methods Appl. Sci. **12** 67-76, 1989. 67–76.

[14] R. Gilbert, Y. Xu, *Starting fields and far fields in ocean acoustics*, Wave Motion **11** 507-524, 1989.

[15] R. Gilbert and Y. Xu, *The propagation problem and far-field pattern in a stratified finite-depth ocean*, Math. Methods Appl. Sci. **12** 199-208, 1990.

[16] R. Gilbert and Y. Xu, *Acoustic waves and far-field patterns in two-dimensional oceans with porous-elastic seabeds*, Results Math. **22** 685–700, 1992.

[17] R. Gilbert and Y. Xu, *The seamount problem*, Nonlinear problems in applied mathematics, 140-149, SIAM, Philadelphia, PA, 1996.

[18] R. Gilbert, Y. Xu and P. Thejll, *An approximation scheme for the three dimensional scattered wave and its propagating far field pattern in a finite depth ocean*, J. Appl. Math. Mech. **72** 459-480, 1992.

[19] R. Gilbert, M. Wirby and Y. Xu, *Determination of a buried object in a two-layered shallow ocean*, J. Comput. Acoust. **9** 1025-1037, 2001.

[20] R. Gilbert and Y. Xu, *Acoustic imaging in a shallow ocean with a thin ice cap*, Inv. Probl. **16** 1799-1811, 2000.

[21] K. Liu, Y. Xu and J. Zou, *Imaging wave-penetrable objects in a finite depth ocean*, Appl. Math. Comp.**235** 364-376, 2014.

[22] K. Liu, Y. Xu and J. Zou, *A multilevel sampling method for detecting sources in a stratified ocean waveguide*, J. Comput. Appl. Math. **309** 95-110, 2017.

[23] K. Liu, Y. Xu and J. Zou, *Direct recovery of wave-penetrable scatterers in a stratified ocean waveguide*, J. Comput. Appl. Math. **338** 239-257, 2018.

[24] K. Liu, *Direct imaging of inhomogeneous obstacles in a three-layered ocean waveguide*, Commun. Comput. Phys., **26** 700-718, 2018.

[25] K. Liu, *Near-field imaging of inhomogeneities in a stratified ocean waveguide*, J. Comput. Phys. **398** 108901, 2019.

[26] K. Liu, *Fast imaging of sources and scatterers in a stratified ocean waveguide*, SIAM J. Imag. Scien. **14** 224-245, 2021.

[27] Y. Xu, *The propagation solutions and far-field patterns for acoustic harmonic waves in a finite depth ocean*, Appl. Anal. **35** 129–151, 1990.

[28] Y. Xu, *Scattering of acoustic wave by obstacle in stratified medium*, Pitman Research Notes in Mathematics Series **263** 147-168, 1992.

[29] Y. Xu, *Reciprocity Relations and Completeness of Far-field Pattern Vectors for Obstacle Scattering of Acoustic Wave in a Stratified Medium*, Math. Methods Appl. Sci. **18** 51-66, 1995.

[30] Y. Xu, *Radiation condition and scattering problem for time-harmonic acoustic waves in a stratified medium with a nonstratified inhomogeneity*, IMA J. Appl. Math. **54** 9-29, 1995.

[31] Y. Xu, *Object shape determination using incomplete data in a stratified medium*, Proc. SPIE 2756, Automatic Object Recognition VI, 1996.

[32] Y. Xu, *Inverse acoustic scattering problems in ocean environments*, J. Acoust. Soc. Am. **9** 111-132, 1999.

[33] Y. Xu, *Upward radiation condition for wave in essentially stratified medium*, J. Phys.: Conference Series **290** 012019, 2011.

[34] Y. Xu, C. Mawata and W. Lin, *Generalized dual space indicator method for underwater imaging*, Inv. Prob. **16** 1761-1776, 2000.

[35] Y. Xu and Y. Yi, *Source localization processing in perturbed waveguides*, J. Acoust. Soc. Am. **8** 1-16, 1992.

[36] Y. Xu and Y. Yi, *A boundary integral method for acoustic source localization in a waveguide with inclusion*, J. Comput. Acoust. **2** 133-145, 1994.